Theoretical Chemistry Accounts (2019) 138:31
https://doi.org/10.1007/s00214-019-2418-1

REGULAR ARTICLE

Structural, electronic and mechanical properties of single-walled AlN and GaN nanotubes via DFT/B3LYP

Giovanne B. Pinhal[1] · Naiara L. Marana[1] · Guilherme S. L. Fabris[1] · Julio R. Sambrano[1]

Received: 21 August 2018 / Accepted: 14 January 2019 / Published online: 28 January 2019

Abstract

Density functional theory with B3LYP hybrid functional and all-electron basis set was applied to study the AlN (SWAlNNTs) and GaN (SWGaNNTs) single-walled nanotubes.The structural and electronic properties were analyzed in function of its diameter and chiralities. Additionally, the elastic and piezoelectric constants were calculated for armchair, zigzag and chiral nanotubes. The simulations showed that both, SWAlNNTs and SWGaNNTs, are easily formed from the graphene-like surface than from the respective bulk. As the diameter increases, the band gap energy also increases, but converges to the band gap energy of its precursor surface. The calculated elastic constants for bulk, graphene-like surface and nanotubes of AlN and GaN show that AlN, in all configurations, is more rigid than GaN. This effect can be related to the more pronounced ionic character of Al–N bond, which confers the stiffness of material. This stiffness affects the AlN nanotube formation, especially that with small diameter, that has the higher energy strain and formation energy for all chiralities. The AlN configurations have piezoelectric response ~25% greater than GaN. The AlN zigzag nanotube has the higher piezoelectric constant e_{11}, i.e., 0.84 C/m^2. Compared to AlN bulk, the e_{11} of nanotube is less than the e_{33} of its bulk, 1.44 C/m^2, but is higher when compared with the others' piezoelectric constants of bulk and surface. Therefore, although the nanotubes present the same stability in diameters above 20 Å, AlN and GaN differ in their band gap energy, piezoelectric response and elastic constant, which will interfere directly with their application in electronic and piezoelectric devices, besides a possible functionalization, such as doping or molecule adsorption.

Keywords Nanotube · Piezoelectric response · GaN · AlN

1 Introduction

In the last decades, the nanotubes have been prominent since the discovery of carbon nanotubes by Iijima [1, 2], where several researches have emerged, aiming at the development and applications of such nanotubes. However, nanotubes of inorganic materials began to be studied, once the electrical properties of carbon nanotubes are dependent on the chirality obtained (where armchair nanotubes are always metallic, while zigzag and chiral nanotubes can be metallic or semiconducting), which make it difficult to be applied in semiconductor devices. Among the inorganic nanotubes, the aluminum and gallium nitrides (AlN and GaN, respectively) present some interesting characteristics, such as hydrogen storage capacity, high electronic mobility, good dielectric properties and thermal conductivity [3, 4], and can be used in electronic devices such as optoelectronics, spintronic semiconductors, gas sensors and nanoscale molecular sensors [5].

The thermodynamically stable phase of AlN and GaN under normal conditions is the hexagonal wurtzite structure ($P6_3mc$ space group). They are considered a wide-band-gap semiconductor, with the band gap of ~3.5 eV [6–8] and ~6.3 eV [9, 10], for GaN and AlN, respectively. These materials can be synthesized by metalorganic chemical vapor deposition (MOCVD), molecular beam epitaxy, hydride vapor-phase epitaxy [6], and can use AlN/SiC as a substrate in a solution with Al/Li_3N [11]. Due to their electronic properties, GaN and AlN have attracted the

Electronic supplementary material The online version of this article (https://doi.org/10.1007/s00214-019-2418-1) contains supplementary material, which is available to authorized users.

✉ Julio R. Sambrano
jr.sambrano@unesp.br

[1] Modeling and Molecular Simulation Group - CDMF, São Paulo State University, UNESP, Bauru, SP 17033-360, Brazil

attention of many researchers due to their diverse application in electronic devices, such as optoelectronics, LEDs, quantum-point lasers, lasers that range from red to ultraviolet, transistors and others [12–14]. More broadly, the AlN has different applications due to its greater piezoelectricity, which increases the chances of application on micro-transducers for ultrasound [15–17].

In particular, some theoretical studies of AlN and GaN nanotubes were carried out and pointed interesting features. Theoretical simulations show that the GaN armchair nanotube configuration is the most stable of all three chiralities due to the homogeneous distribution of charges on the surfaces [18]. Young's modulus of GaN nanotubes undergoes little change regarding the diameter increase, and its value is lower than the bulk value and higher than the surface [19]. In addition, due to the contribution of d orbitals of the gallium atoms, the stabilization of the nanotube grow occurs, and this enables the application in spintronics by introducing transition metals in the nanotube [20].

AlN nanotubes appear to be efficient as toxic gas sensors [4], in CO adsorption [21], removal of ethylacetylene from the environment [22] and as formaldehyde sensor [23], which can be detected by changes in the electrical conductivity of nanotubes. Moreover, it was observed that physisorption of CO_2 and N_2 molecules is poorly affected by the nanotube diameter [24]. Furthermore, the adsorption introduces certain defects on the structure and the nanotube can change from semiconductor to conductor, being able to be used in magneto-electronics [25].

Therefore, even though there are previous research papers about the AlN and GaN nanotubes, a detailed work of the influence of the nanotube diameter on their properties is essential. Moreover, AlN and GaN bulks are known for their piezoelectricity and, to our knowledge, there are no reports in the literature exploring the piezoelectric constants of those two nanotubes. In this sense, the aim of this work is to investigate the properties of the single-walled AlN (SWAlNNTs) and GaN (SWGaNNTs) nanotubes with different diameters through periodic density functional theory (DFT) calculations. The structural and electronic properties, as well as the elastic and piezoelectric constants, are explored and discussed. The purpose of this article is to show and guide future research as to the feasibility of applying this material.

2 Theoretical methods

Periodic DFT calculations with the B3LYP hybrid functional [26] were taken using the CRYSTAL17 computer code [27]. CRYSTAL uses Gaussian-type basis set to represent crystalline orbital as a linear combination of Bloch functions defined in terms of local functions (atomic orbital).

The aluminum, gallium and nitrogen centers were described by 86-21G* [28], 86-4111d41G [29] and 6-21G* [30], respectively. The level of calculation accuracy for the Coulomb and exchange series was controlled by five-threshold set (10^{-8}, 10^{-8}, 10^{-8}, 10^{-8} and 10^{-16}). These parameters represent the overlap and penetration for Coulomb integrals, the overlap for HF exchange integrals and the pseudo-overlap (HF exchange series), respectively. The shrinking factor (Pack–Monkhorst and Gilat net) was set to 10, corresponding to 6 independent k-points in the irreducible part of the Brillouin zone integration.

The band structures were obtained for 100 k-points along the appropriate high symmetry paths of the adequate Brillouin zone, and the diagrams of the density of states (DOS) were calculated for analysis of the corresponding electronic structure. The choice of a theoretical exploration of these systems is based on the previous work by our research group [31–33].

The elastic and piezoelectric constants were calculated using the methodology implemented in the CRYSTAL code. This methodology was previously extensively tested for 3D systems (see ref [34, 35]). However, it is important to emphasize that in the particular case of 1D systems, the volume of the nanotube in the elastic constant equation is taken as $V = 2\pi R\left|\vec{L}\right|l$, where R is the nanotube radius, $\left|\vec{L}\right|$ is the nanotube length calculated by $\left|\vec{L}\right| = l_1 a_1 + l_2 a_2$, where a_1 and a_2 are the slab cell vectors which are used to roll up the nanotubes and l_1 and l_2 are integers, and l is the nanotube thickness (of single-walled nanotube corresponding to the atom diameter). This method was successfully applied to calculate the elastic constants of other nanotube models [31]. Because of the single-direction periodicity, the elastic and piezoelectric response are along the periodic direction of the nanotube, i.e., along the C_{11} and e_{11} components, respectively.

The Mulliken charges were calculated for all the atoms of optimized models. The Hirshfeld-I method was reconfigured from the original Hirshfeld scheme [36], which eliminates the need of calculating the promolecular density by replacing them with spherical symmetric weight functions, optimized through an iterative procedure. Both methods are implemented in the CRYSTAL program [37].

3 Computational models

The AlN and GaN in the hexagonal wurtzite phase can be depicted as alternating planes of tetrahedral coordinated with N^{3-} ions surrounded by Al^{3+} or Ga^{3+} ions, forming an $[AlN_4]$ and $[GaN_4]$ cluster and stacked alternately along the c-axis. The wurtzite structure has two external parameters, a and c, and one internal coordinate u, which corresponds to the N position with respect to Al or Ga. This structure

produces an accumulating normal dipole moment, which turns it prop to the piezoelectricity.

At the first step, the bulk equilibrium structures of AlN and GaN were determinate; their total energies were optimized with respect to the lattice parameters and the internal coordinate. From the optimized bulk parameters, the monolayer (0001) surfaces were constructed and re-optimized with respect to their atomic positions and cell parameters. Then, the relaxed monolayer surfaces were rolled up, generating the single-walled (SW) armchair, zigzag and chiral nanotubes, and were fully re-optimized. Depending on the direction of the rolling sheet, the nanotubes can be classified as armchair (n, n), zigzag (n, 0) and chiral nanotubes (n, m), where the integers n and m determine the diameter and chirality of the nanotube (see Fig. 1).

4 Results

The previously calculated optimized AlN bulk parameters are $a=3.122$ Å, $c=4.994$ Å and $u=0.381$, which correspond to 0.38%, 0.28% and 0.26%, respectively, deviation from experimental values [38]. The optimized lattice parameters for GaN bulk are $a=3.212$ Å, $c=5.204$ Å and $u=0.377$, with 0.69%, 0.29% and 0.00%, respectively, from experimental values [39]. Both AlN and GaN bulk parameters are in agreement with the experimental data, and the level of theory applied is consistent for describing the structural properties of the material [40, 41].

Tables 1 and 2 report the theoretical optimized diameter, nanotube length, average bond length (and overlap population), average bond angle, Mulliken charges, E_{gap}, E_s and E_{form} of SWAlNNTs and SWGaNNTs.

The geometrical structures of both nanotubes chiralities became similar to the (0001) monolayer surfaces as the nanotube diameter increases [40]. This behavior is a characteristic perceived by all single-walled nanotubes with larger diameter [33]. However, even nanotubes with smaller diameter maintain the (0001) monolayer surfaces characteristics. Although they present a particular behavior, the bonds Al–N and Ga–N are more ionic, the strain energies and formation energies are greater and the band gap is smaller when compared to nanotubes with large diameter. This performance may be caused by the interactions between the atoms of the nanotube cavity, which lead to high E_s and low stability.

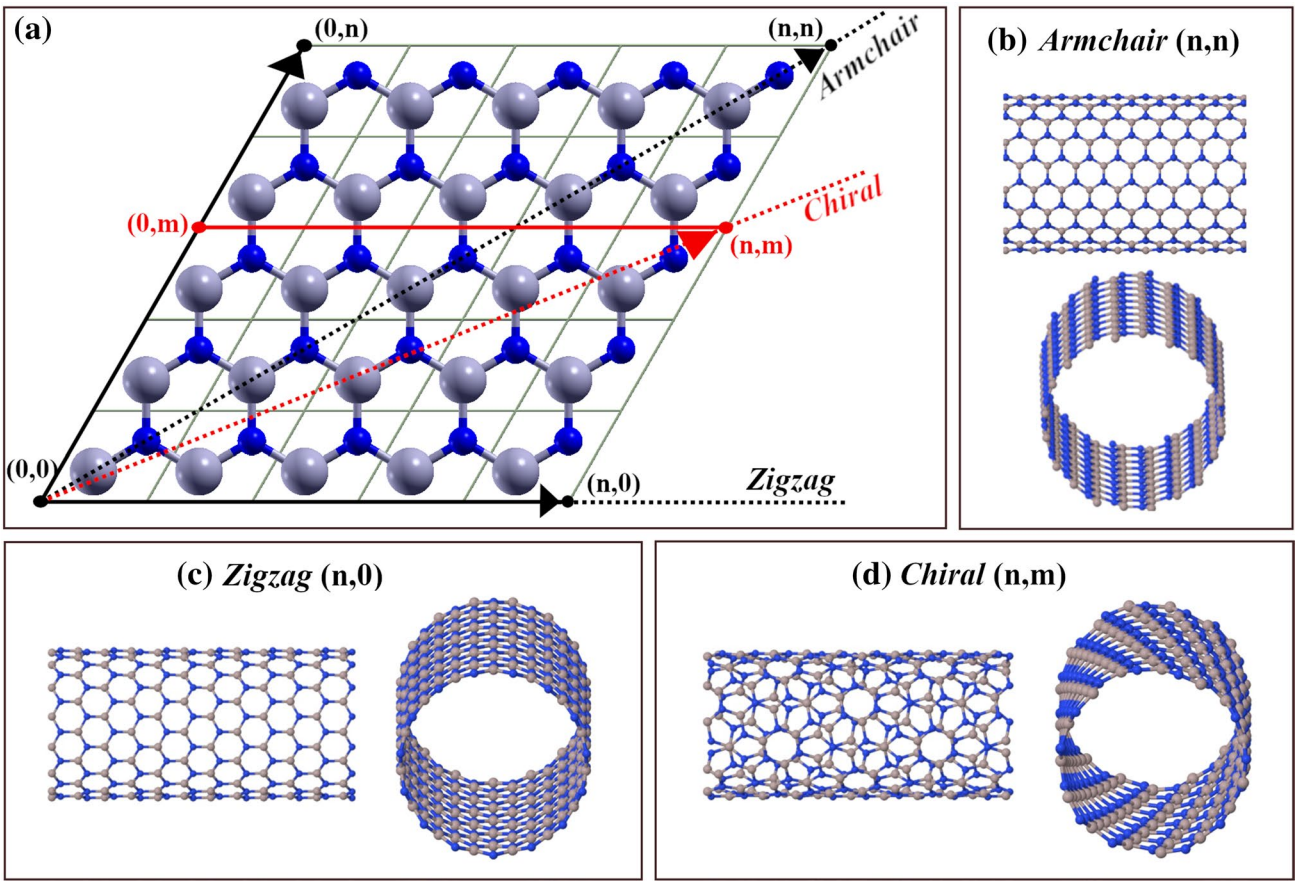

Fig. 1 Scheme for generic single-walled nanotube construction **a** from a monolayer surface forming structures with **b** armchair (n, n), **c** zigzag (n, 0) and **d** chiral (n, m) symmetries

Table 1 Number of atoms in the nanotube (n_{NT}), nanotube diameter (D; Å), nanotube length ($|\vec{L}|$; Å), average Al–N bond length (Å), overlap population (m|e|), average Al–N̂–Al bond angle (°), Mulliken charges (Q), band gap energy (E_{gap}; eV), strain energy (E_s; eV/atom) and formation energy (E_{form}; eV/atom) of SWAlNNTs

	n_{nt}	D	$\lvert\vec{L}\rvert$	Al–N (overlap)	Al–N̂–Al	Q	E_s	E_{form}	E_{gap}
Armchair									
(5,5)	20	8.57	3.11	1.79 (0.298)	118.73	1.145	0.09	1.55	6.26
(10,10)	40	17.10	3.10	1.79 (0.301)	119.67	1.153	0.03	1.48	6.52
(15,15)	60	25.64	3.10	1.79 (0.301)	119.83	1.154	0.01	1.47	6.57
(20,20)	80	34.18	3.10	1.79 (0.301)	119.93	1.155	0.00	1.46	6.59
(25,25)	100	42.72	3.10	1.79 (0.301)	119.97	1.155	0.00	1.46	6.60
(50,50)	200	85.44	3.10	1.79 (0.301)	120.00	1.155	0.00	1.46	6.61
(100,100)	400	170.87	3.10	1.79 (0.301)	120.00	1.156	0.00	1.46	6.62
Zigzag									
(5,0)	20	5.15	5.25	1.80 (0.291)	116.15	1.123	0.32	1.78	4.89
(10,0)	40	9.96	5.34	1.79 (0.299)	119.02	1.147	0.07	1.53	6.32
(15,0)	60	14.86	5.36	1.79 (0.300)	119.58	1.152	0.03	1.49	6.49
(20,0)	80	19.78	5.36	1.79 (0.301)	119.75	1.154	0.00	1.46	6.58
(40,0)	160	39.46	5.37	1.79 (0.301)	119.93	1.155	0.00	1.46	6.59
(50,0)	200	49.35	5.37	1.79 (0.301)	119.98	1.155	0.00	1.46	6.59
(80,0)	320	78.92	5.37	1.79 (0.301)	120.00	1.155	0.00	1.46	6.60
(100,0)	400	98.66	5.37	1.79 (0.301)	120.00	1.155	0.00	1.46	6.60
(120,0)	480	118.38	5.37	1.79 (0.301)	120.00	1.156	0.00	1.46	6.60
Chiral									
(4,3)	148	6.04	32.87	1.80 (0.294)	117.52	1.133	0.20	1.65	5.98
(5,3)	196	6.96	37.68	1.79 (0.296)	118.07	1.138	0.15	1.60	6.09
(6,3)	84	7.88	14.21	1.79 (0.297)	118.48	1.142	0.11	1.57	6.20
(5,4)	244	7.73	42.09	1.79 (0.297)	118.43	1.142	0.12	1.57	6.22
(6,4)	152	8.63	23.45	1.79 (0.298)	118.73	1.145	0.09	1.55	6.27
(7,4)	124	9.55	17.23	1.79 (0.299)	118.97	1.147	0.08	1.53	6.33
(8,4)	112	10.48	14.21	1.79 (0.299)	119.15	1.148	0.06	1.52	6.39
(6,5)	364	9.43	51.34	1.79 (0.300)	118.95	1.149	0.08	1.53	6.34
(7,5)	436	10.33	56.14	1.79 (0.299)	119.13	1.148	0.07	1.52	6.37
(8,5)	172	11.23	20.34	1.79 (0.300)	119.25	1.150	0.06	1.51	6.40
(9,5)	604	12.15	66.00	1.79 (0.300)	119.37	1.150	0.05	1.50	6.44
(10,5)	140	13.08	14.20	1.79 (0.300)	119.45	1.151	0.04	1.50	6.46
(11,10)	1324	17.97	97.72	1.79 (0.301)	119.72	1.153	0.02	1.48	6.53
(12,10)	728	18.84	51.24	1.79 (0.301)	119.72	1.153	0.04	1.50	6.53
(13,10)	532	19.72	35.76	1.79 (0.301)	119.77	1.153	0.02	1.48	6.54
(14,10)	872	20.61	56.07	1.79 (0.301)	119.82	1.154	0.02	1.47	6.55
(15,10)	380	21.52	23.40	1.79 (0.301)	119.82	1.154	0.02	1.47	6.55
(16,10)	344	22.43	20.33	1.79 (0.301)	119.85	1.154	0.02	1.47	6.55
(18,10)	1208	24.27	65.97	1.79 (0.301)	119.87	1.154	0.01	1.47	6.56
(19,10)	868	25.19	45.66	1.79 (0.301)	119.87	1.154	0.01	1.47	6.56
(20,10)	280	26.12	14.20	1.79 (0.301)	119.87	1.154	0.01	1.47	6.57
(40,20)	560	52.22	14.20	1.79 (0.301)	119.97	1.155	0.00	1.46	6.59

It should be noted that Mulliken charges, Q, are showed in modulus (i.e., in absolute values, the positive aluminum and gallium charge and negative nitrogen charge have the same value). It was observed that the nanotubes with small diameter present minor charges than greater diameter nanotubes; however, the charges also converge for nanotubes with diameter above 20 Å, in ~ 1.16 and 1.12 au for AlN and GaN, respectively. Although the AlN nanotubes exhibit a greater charge of their atoms, as a whole, the nanotubes are neutral (as well as GaN), i.e., the sum of the atoms charges of all system is zero. For comparison, the Hirshfeld-I charges analysis was performed. The calculated values for all models of AlN and GaN nanotubes were 1.71 and 1.28 au, respectively. Both nanotubes present Mulliken and Hirshfeld-I atomic charges very close to the (0001) monolayer surface. Compared with bulk charges, the difference is around

Table 2 Number of atoms in the nanotube (n_{NT}), nanotube diameter (D; Å), nanotube length ($|\vec{L}|$; Å), average Ga–N bond length (Å), overlap population (*mle*), average Ga–N̂–Ga bond angle (°), Mulliken charges (Q), band gap energy (E_{gap}; eV), strain energy (E_s; eV/atom) and formation energy (E_{form}; eV/atom) of SWGaNNTs

	n_{nt}	D	$\lvert\vec{L}\rvert$	Ga–N (overlap)	Ga–N̂–Ga	Q	E_s	E_{form}	E_{gap}
Armchair									
(5,5)	20	8.85	3.20	1.85 (0.291)	118.57	1.002	0.08	1.38	4.42
(10,10)	40	17.64	3.19	1.85 (0.297)	119.64	1.010	0.03	1.32	4.59
(15,15)	60	26.43	3.19	1.84 (0.298)	119.87	1.012	0.01	1.31	4.63
(20,20)	80	35.24	3.19	1.84 (0.298)	119.93	1.012	0.00	1.30	4.64
(25,25)	100	44.02	3.19	1.84 (0.298)	119.97	1.012	0.00	1.30	4.65
(50,50)	200	88.06	3.19	1.84 (0.298)	119.97	1.013	0.00	1.30	4.66
(100,100)	400	176.09	3.19	1.84 (0.298)	120.00	1.013	0.00	1.30	4.66
Zigzag									
(5,0)	20	5.31	5.42	1.86 (0.281)	115.90	0.976	0.30	1.60	4.01
(10,0)	40	10.26	5.51	1.85 (0.294)	118.94	1.004	0.07	1.36	4.51
(15,0)	60	15.31	5.52	1.85 (0.296)	119.50	1.009	0.03	1.33	4.56
(20,0)	80	20.38	5.53	1.84 (0.297)	119.72	1.011	0.00	1.30	4.63
(40,0)	160	40.66	5.53	1.84 (0.298)	119.93	1.012	0.00	1.30	4.63
(50,0)	200	50.85	5.53	1.84 (0.298)	120.00	1.012	0.00	1.30	4.64
(80,0)	320	81.33	5.53	1.84 (0.298)	119.98	1.013	0.00	1.30	4.64
(120,0)	480	121.99	5.53	1.84 (0.298)	120.00	1.013	0.00	1.30	4.64
Chiral									
(4,3)	148	6.26	33.72	1.85 (0.288)	117.27	0.989	0.18	1.48	4.25
(5,3)	196	7.19	38.73	1.85 (0.287)	117.87	0.995	0.13	1.43	4.32
(6,3)	84	8.14	14.63	1.85 (0.289)	118.34	0.999	0.10	1.40	4.38
(5,4)	244	7.99	43.27	1.85 (0.289)	118.30	0.999	0.10	1.40	4.40
(6,4)	152	8.92	24.13	1.85 (0.291)	118.63	1.002	0.08	1.38	4.44
(7,4)	124	9.85	17.78	1.85 (0.292)	118.85	1.004	0.07	1.36	4.46
(8,4)	112	10.81	14.63	1.85 (0.294)	118.48	1.005	0.06	1.36	4.51
(6,5)	364	9.74	52.83	1.85 (0.292)	118.62	1.004	0.07	1.37	4.48
(7,5)	436	10.66	57.78	1.85 (0.293)	119.03	1.005	0.06	1.35	4.50
(8,5)	172	11.59	20.95	1.85 (0.295)	119.17	1.006	0.05	1.35	4.51
(9,5)	604	12.54	67.97	1.85 (0.295)	119.30	1.007	0.05	1.34	4.54
(10,5)	140	13.49	14.64	1.85 (0.295)	119.28	1.008	0.04	1.34	4.55
(11,10)	1324	18.53	100.66	1.84 (0.297)	119.67	1.010	0.02	1.32	4.59
(12,10)	728	19.42	52.78	1.84 (0.297)	119.77	1.010	0.02	1.32	4.59
(13,10)	532	20.33	36.84	1.84 (0.297)	119.72	1.011	0.02	1.32	4.60
(14,10)	872	21.25	57.77	1.84 (0.297)	119.75	1.011	0.02	1.32	4.60
(15,10)	380	22.18	24.12	1.84 (0.297)	119.75	1.011	0.02	1.31	4.61
(16,10)	344	23.12	20.94	1.84 (0.297)	119.78	1.011	0.02	1.31	4.61
(18,10)	1208	25.01	67.98	1.84 (0.297)	119.87	1.011	0.01	1.31	4.61
(19,10)	868	25.96	47.05	1.84 (0.297)	119.82	1.011	0.01	1.31	4.61
(20,10)	280	26.92	14.64	1.84 (0.297)	119.82	1.012	0.01	1.31	4.62
(40,20)	560	53.81	14.64	1.84 (0.298)	119.97	1.012	0.00	1.30	4.64

0.09 au and 0.03 au, for AlN and GaN, respectively. Thus, the charge difference presented between the AlN and GaN may influence in a possible functionalization, such as doping, adsorption, among others.

In connection herewith, the analysis of E_s and E_{form} helps predict the preferential chirality formation. Figure 2 illustrates the relationship between E_s, E_{form} and E_{gap} as functions of the diameter for SWAlNNTs and SWGaNNTs with different chiralities.

In general, the calculated E_{form} is higher than E_s for all nanotube types, suggesting that nanotubes are more easily formed from the monolayer surface than from the bulk. The increase in nanotube diameter showed a decrease in E_s and E_{form}. However, it is observed that both energies converge from (20,20), (20,0) and (11,10) nanotubes, i.e., for nanotubes with nanotube diameter up to 20 Å. In the case of the chiral nanotubes, E_s and E_{form} had not presented a very clear convergence, even for those nanotubes with the

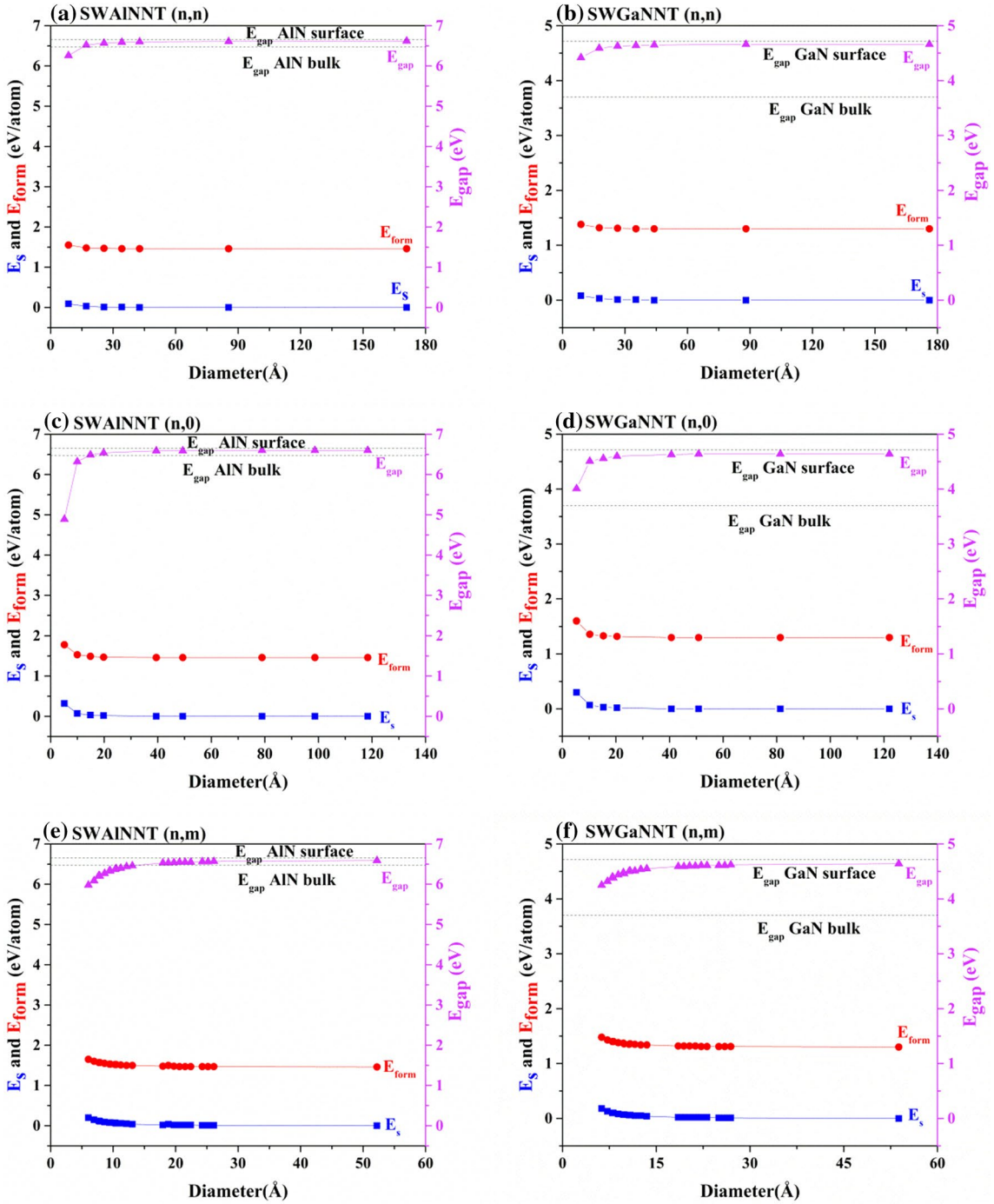

Fig. 2 E_s (eV/atom), E_{form} (eV/atom) and E_{gap} as a function of the diameter (Å) for **a** armchair (n, n) SWAlNNTs, **b** armchair (n, n) SWGaNNTs, **c** zigzag (n, 0) SWAlNNTs, **d** zigzag (n, 0) SWGaNNTs, **e** chiral (n, m) SWAlNNTs, **f** chiral (n, m) SWGaNNTs

same chiral angle, such as (6,3), (8,4), (10,5), (20,10) and (40,20) ($\theta = 19.11°$), which differ in 0.10 eV/atom of E_s for (6,3) and (40,20). These results showed that nanotubes with a small diameter can be more difficult to obtain than those with larger diameters. In general, E_s was 0.0 eV/atom for AlN and GaN nanotubes, while the E_{form} was 1.46 eV/atom and 1.30 eV/atom, for AlN and GaN nanotubes, respectively, suggesting that both nanotubes are formed the same way from the surfaces. Therefore, the three types of AlN and GaN nanotubes can be equally formed for diameters up to 20 Å.

The same behavior was observed for different materials, including ZnO and carbon nanotubes, although ZnO, GaN and AlN present E_s and E_{form} minor than carbon nanotubes

[33], which suggests that inorganic nanotubes are more easily obtained than SWCNTs.

AlN and GaN are quite conceptualized semiconductors employed in the most diverse devices, as pointed out previously. Their nanotubes have the semiconductor characteristic with E_{gap} around 6.54 eV and 4.63 eV, for all SWAlNNTs and SWGaNNTs, respectively. Both nanotubes are considered a wide-band-gap semiconductor and presented a deviation of around + 0.34 eV and + 1.12 eV from the experimental band gap of AlN and GaN bulk, respectively [9]. The region of the electromagnetic spectrum also changed for the nanotubes, with both emitting on deep UV, while for the GaN bulk the emission region is near UV. In addition, the increase in diameter of nanotubes leads to an increase in E_{gap}, which also converges from 20 Å of nanotube diameter for all SWAlNNTs and SWGaNNTs. Besides that, the E_{gap} of nanotubes converges to the E_{gap} of the monolayer (0001) surface, indicating that not only the structural properties are similar to the surface but also the electronic properties.

As the convergence of the main properties analyzed starts from 20 Å of diameter for all chiralities, the nanotubes (20,20), (20,0) and (20,10) are used for the description of the electronic properties and analysis of the elastic and piezoelectric constants.

The electronic properties are discussed based on the band structure and DOS and are shown in Figs. 3, 4, 5 and 6, respectively. The band structure behavior of both nanotubes showed concentrated bands around the band gap and, for the chiral and zigzag nanotubes, showed a flatter valence band, which can suggest a lower mobility of the electrons. According to previous works about semiconductor nanotubes, the flatter bands around the band gap are a characteristic of these nanotubes, which are in contrast with the band structures of armchair nanotubes [32, 33]. For all AlN nanotubes, the band gap is direct at Γ point, while for the GaN nanotubes, the armchair presents an indirect band gap between Γ and X. This behavior of armchair GaN nanotube is in contrast with the character of the GaN bulk and monolayer surface, both presenting a direct gap at Γ point (see Figure S1).

With respect to the DOS in Fig. 5, the AlN nanotubes present a classical contribution for the semiconductor material around the band gap region: the anion (N) contributes on

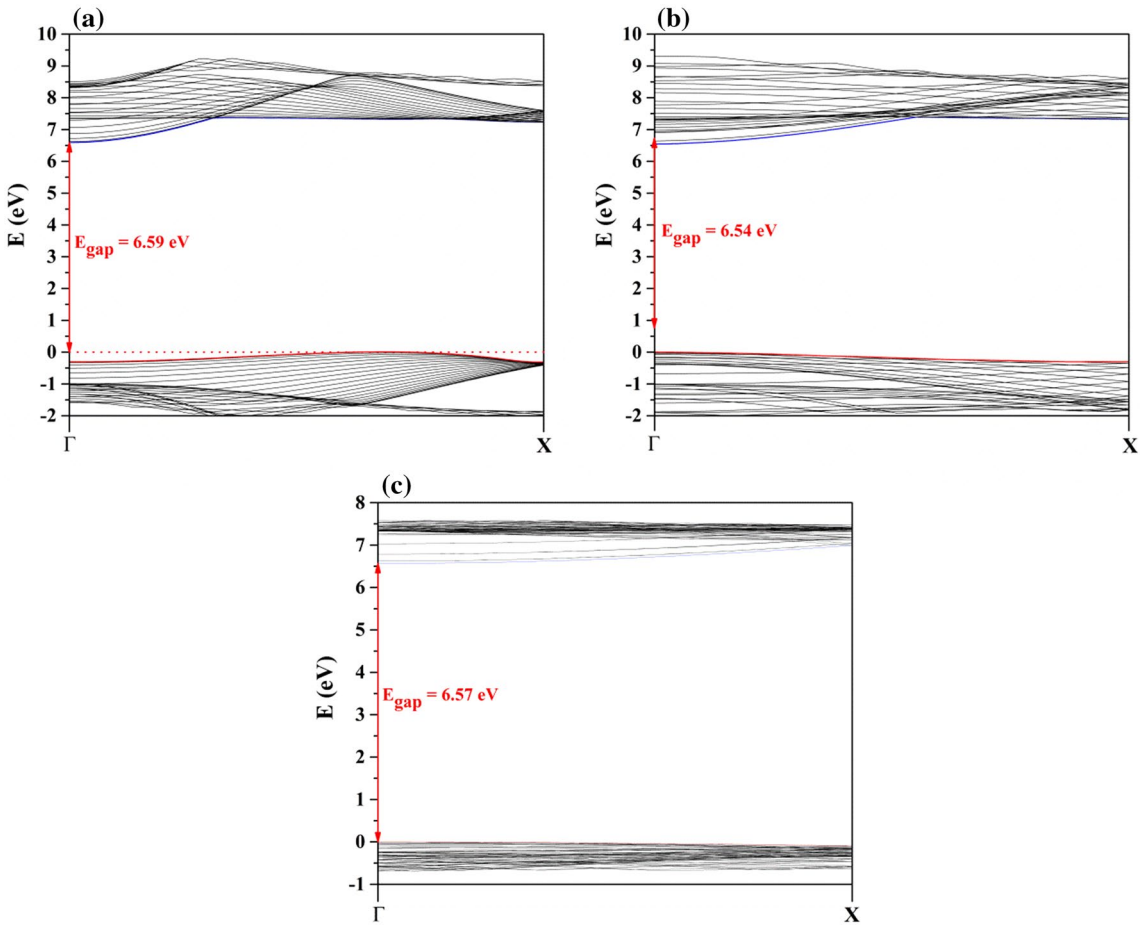

Fig. 3 Band structure of **a** (20,20), **b** (20,0) and (c) (11,10) single-walled AlN nanotubes

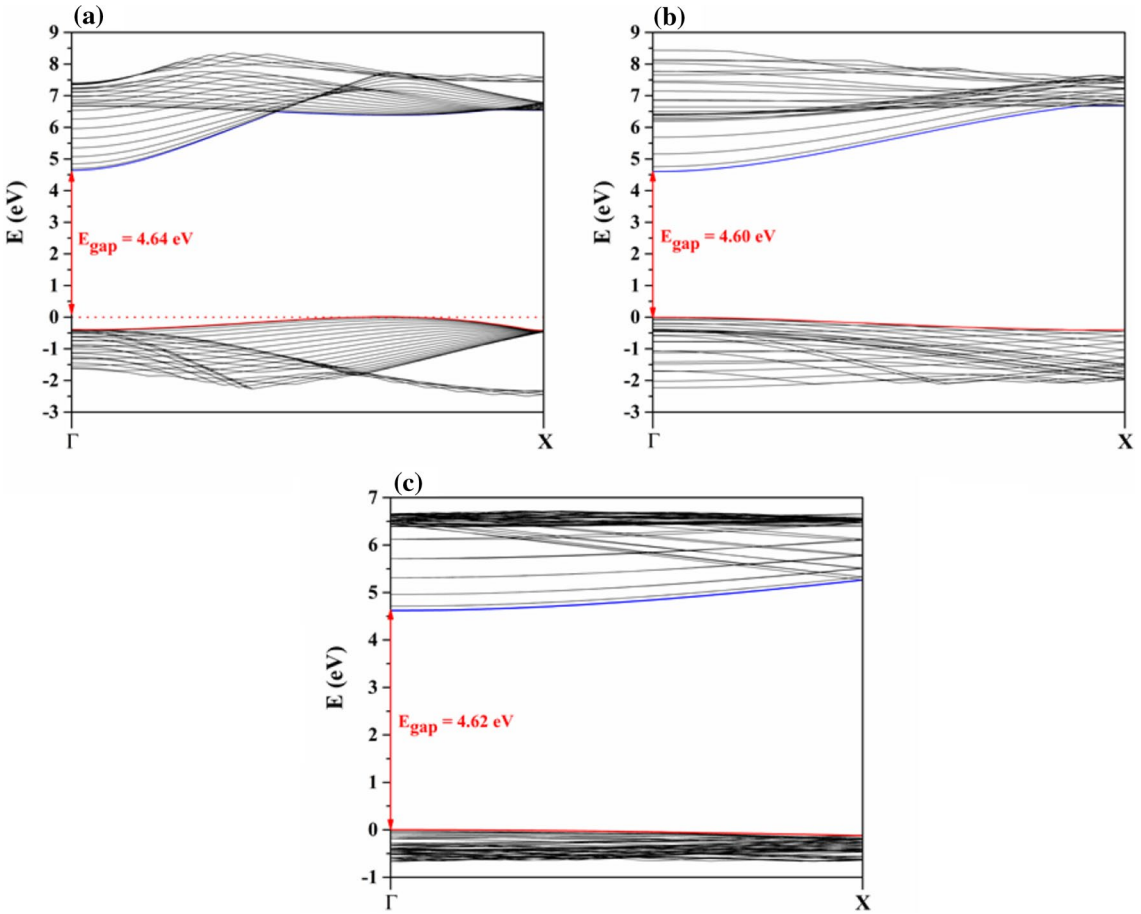

Fig. 4 Band structure of **a** (20,20), **b** (20,0) and **c** (11,10) single-walled GaN nanotubes

valence band and the cation (Al) contributes on conduction band. For both atoms, in all AlN nanotubes, the p_y and p_z orbitals are degenerated and appear as p_yp_z. The p_yp_z orbitals of N atoms present the major contribution on valence band, while the p_x contribution is relevant at inner valence bands. At conduction band, the *s* orbital of Al atoms presents the major contribution immediately at gap region; however, the major contribution is p_yp_z orbitals along the conduction band. All the three chiralities of AlN nanotubes showed similar contribution compared with the bulk and monolayer surface, although the contribution on bulk is more "scattered" along the valence and conduction bands. Therefore, the electron transition occurs between N-p_yp_z and Al-*s*.

A similar behavior is observed for the GaN nanotubes (Fig. 6): N atoms contribute on valence band and Ga atoms contribute on conduction band. At valence band, the 3d orbitals of Ga atoms present a small contribution at inner bands, while the major contributor at band gap region on conduction band is also the *s* orbitals and at inner conduction band is p_yp_z orbitals. The N atoms contribute to band gap region with p_yp_z orbitals and to inner conduction band with the same orbitals. Although the armchair SWGaNNTs present an indirect gap, the DOS behavior is similar to the zigzag and chiral nanotubes and kept the characteristic DOS of GaN bulk and monolayer surface (Figure S2). In GaN case, the electron transition occurs between N-p_yp_z and Ga-*s*.

Notwithstanding both AlN and GaN nanotubes presented similarities regarding the structural properties and E_{gap} value with their respective monolayer surfaces, the DOS has slight differences, which show the Al and Ga atoms significantly contributing to both valence and conduction bands.

The elastic and piezoelectric constants are calculated (Table 3) for all nanotube chiralities, and the values were compared with their respective bulk values. In general, armchair nanotubes are more rigid than zigzag and chiral nanotubes; however, on SWGaNNTs the difference is more evident, where armchair is ~ 17 GPa more rigid, while on SWAlNNTs the difference is only 6 GPa for armchair in comparison with zigzag. According to Table 3, the elastic constant of SWAlNNTs is 19.95 GPa greater than SWGaNNTs, showing that AlN nanotubes are more rigid than GaN nanotubes, which are in agreement with the C_{11}, C_{44} and bulk modulus obtained for the bulk (see Supplemental Material). The stiffness of AlN nanotubes, also

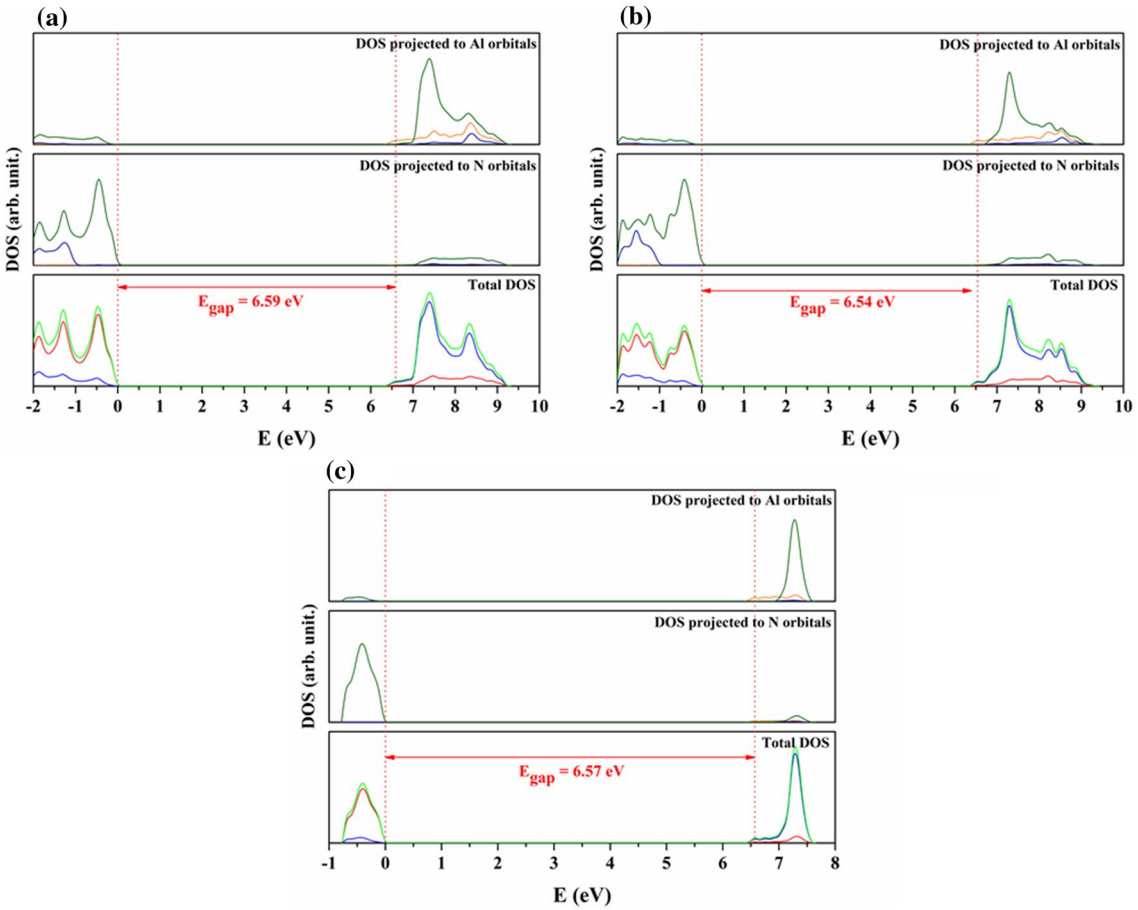

Fig. 5 DOS of **a** (20,20), **b** (20,0) and **c** (11,10) single-walled AlN nanotubes

observed for bulk, may be related to higher E_{form} and also E_s for smaller nanotubes; thus, the greater the elastic constant for the material, the greater will be the energy expended to obtain the corresponding nanotube. Additionally, the AlN presents more ionic bond than GaN, which can also influence the elastic constant behavior and its stiffness.

As shown in previous works, the armchair nanotubes did not present any piezoelectric response [42, 43]. On the other hand, the zigzag nanotubes of both materials are a potential piezoelectric material, with piezoelectric response higher than chiral nanotubes. The piezoelectric response occurs in the same direction of the tension applied, i.e., along the periodic direction. Although SWAlNNTs are more rigid, these nanotubes had a larger piezoelectric response when compared to the SWGaNNTs; the difference is ~25%, and it follows the same trend as presented by the bulk. The e_{11} constant for the zigzag SWAlNNTs is 43%, −0.38% and −0.73% different compared with the e_{33}, e_{31} and e_{15} piezoelectric constant for AlN bulk, which indicates that the nanotubes application in piezoelectric devices is as advantageous as the AlN bulk (see Tables S1–S3).

5 Conclusion

Aluminum and gallium nitride nanotubes were analyzed via DFT/B3LYP based on their structural, electronic and mechanical properties. The simulations reveal that both nanotubes resemble the structural geometry of their respective monolayer surfaces as the nanotube diameter increases. Nanotubes with larger diameter are obtained with the same facility from the monolayer surfaces, regardless of nanotube chirality. Although the nitride nanotubes present the same structural characteristic, their electronic properties differ considerably. Both nanotubes converge on the band gap value of the monolayer surface, for nanotubes diameter up to 20 Å; however, the SWAlNNTs present a band gap of 1.94 eV above the SWGaNNTs. This substantial difference can lead to different applications on electronic devices. In addition, SWAlNNTs have higher values of piezoelectric response, being as efficient as their respective bulk, which can perfectly replace the bulk by nanotubes on piezotronics devices.

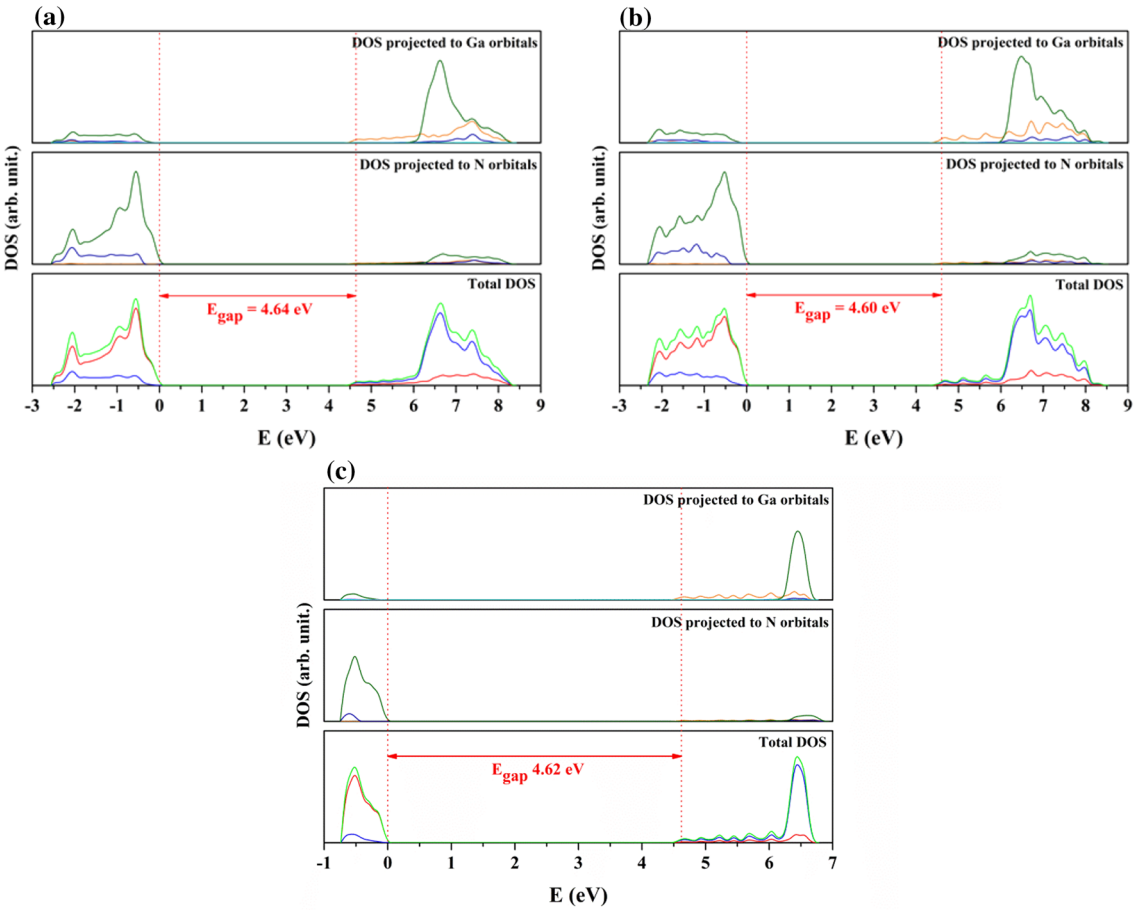

Fig. 6 DOS of **a** (20,20), **b** (20,0) and **c** (11,10) single-walled GaN nanotubes

Table 3 Elastic (C_{11}, GPa) and piezoelectric (e_{11}, C/m^2) constants of single-walled AlN (SWAlNNTs) and GaN (SWGaNNTs) nanotubes

	C_{11}	e_{11}
SWAlNNTs		
(20,0)	387.31	0.83
(20,20)	393.34	–
(20,10)	392.42	0.44
SWGaNNTs		
(20,0)	367.46	0.62
(20,20)	383.70	–
(20,10)	371.07	0.33

Acknowledgements This work is supported by Brazilian Funding Agencies: CAPES (8881.068492/2014-01, 787027/2013), FAPESP (2016/07476-9, 2016/25500-4 and 2013/07296-2). The computational facilities were supported by resources supplied by Molecular Simulations Laboratory, São Paulo State University, Bauru, Brazil.

References

1. Iijima S (1991) Helical microtubules of graphitic carbon. Nature 354:56–58. https://doi.org/10.1038/354056a0
2. Iijima S, Ichihashi T (1993) Single-shell carbon nanotubes of 1-nm diameter. Nature 363:603–605. https://doi.org/10.1038/363603a0
3. Baei MT, Peyghan AA, Bagheri Z (2013) Fluorination of the exterior surface of AlN nanotube: a DFT study. Superlattices Microstruct 53:9–15. https://doi.org/10.1016/j.spmi.2012.09.010
4. Noei M, Salari AA, Ahmadaghaei N et al (2013) DFT study of the dissociative adsorption of HF on an AlN nanotube. C R Chim 16:985–989. https://doi.org/10.1016/j.crci.2013.05.007
5. Li H, Liu C, Liu G et al (2014) Single-crystalline GaN nanotube arrays grown on c-Al_2O_3 substrates using InN nanorods as templates. J Cryst Growth 389:1–4. https://doi.org/10.1016/j.jcrysgro.2013.11.066
6. Zou CW, Yin ML, Li M et al (2007) GaN films deposited by middle-frequency magnetron sputtering. Appl Surf Sci 253:9077–9080. https://doi.org/10.1016/j.apsusc.2007.05.037
7. Lei T, Ludwig KF, Moustakas TD (1993) Heteroepitaxy, polymorphism, and faulting in GaN thin films on silicon and sapphire substrates. J Appl Phys 74:4430–4437. https://doi.org/10.1063/1.354414
8. Maruska HP, Tietjen JJ (1969) The preparation and properties of vapor-deposited single-crystal-line GaN. Appl Phys Lett 15:327–329. https://doi.org/10.1063/1.1652845
9. Vurgaftman I, Meyer JR (2003) Band parameters for nitrogen-containing semiconductors. J Appl Phys 94:3675–3696. https://doi.org/10.1063/1.1600519

10. Feneberg M, Leute RAR, Neuschl B et al (2010) High-excitation and high-resolution photoluminescence spectra of bulk AlN. Phys Rev B 82:75208. https://doi.org/10.1103/PhysRevB.82.075208
11. Kangawa Y, Kakimoto K (2010) AlN synthesis on AlN/SiC template using Li–Al–N solvent. Phys Status Solidi Appl Mater Sci 207:1292–1294. https://doi.org/10.1002/pssa.200983566
12. Morkoç H, Strite S, Gao GB et al (1994) Large-band-gap SiC, III–V nitride, and II–VI ZnSe-based semiconductor device technologies. J Appl Phys 76:1363–1398. https://doi.org/10.1063/1.358463
13. Arakawa Y (2001) Progress in quantum dots for optoelectronics applications. Photonics Technol 21st Century 4598:106–112. https://doi.org/10.1117/12.491501
14. Pérez-Tomás A, Catalàn G, Fontserè A et al (2015) Nanoscale conductive pattern of the homoepitaxial AlGaN/GaN transistor. Nanotechnology 26:115203. https://doi.org/10.1088/0957-4484/26/11/115203
15. Przybyla RJ, Tang H-Y, Shelton SE et al (2014) 12.1 3D ultrasonic gesture recognition. In: IEEE international solid-state circuits conference digest of technical papers. IEEE, pp 210–211
16. Ahmadi Peyghan A, Omidvar A, Hadipour NL et al (2012) Can aluminum nitride nanotubes detect the toxic NH_3 molecules? Phys E Low Dimens Syst Nanostruct 44:1357–1360. https://doi.org/10.1016/j.physe.2012.02.018
17. Taniyasu Y, Kasu M, Makimoto T (2006) An aluminium nitride light-emitting diode with a wavelength of 210 nanometres. Nature 441:325–328. https://doi.org/10.1038/nature04760
18. Sodré JM, Longo E, Taft CA et al (2017) Electronic structure of GaN nanotubes. C R Chim 20:190–196. https://doi.org/10.1016/j.crci.2016.05.023
19. Xu B, Lu AJ, Pan BC, Yu QX (2005) Atomic structures and mechanical properties of single-crystal GaN nanotubes. Phys Rev B 71:125434. https://doi.org/10.1103/PhysRevB.71.125434
20. Zhang M, Shi J-J (2014) Electronic structure and magnetic properties of substitutional transition-metal atoms in GaN nanotubes. Chin Phys B 23:17301. https://doi.org/10.1088/1674-1056/23/1/017301
21. Beheshtian J, Bagheri Z, Kamfiroozi M, Ahmadi A (2012) A theoretical study of CO adsorption on aluminum nitride nanotubes. Struct Chem 23:653–657. https://doi.org/10.1007/s11224-011-9911-z
22. Noei M, Ebrahimikia M, Saghapour Y et al (2015) Removal of ethyl acetylene toxic gas from environmental systems using AlN nanotube. J Nanostruct Chem 5:213–217. https://doi.org/10.1007/s40097-015-0152-3
23. Ahmadi A, Hadipour NL, Kamfiroozi M, Bagheri Z (2012) Theoretical study of aluminum nitride nanotubes for chemical sensing of formaldehyde. Sens Actuators B Chem 161:1025–1029. https://doi.org/10.1016/j.snb.2011.12.001
24. Jiao Y, Du A, Zhu Z et al (2010) A density functional theory study of CO_2 and N_2 adsorption on aluminium nitride single walled nanotubes. J Mater Chem 20:10426. https://doi.org/10.1039/c0jm01416h
25. Zhao M, Xia Y, Liu X et al (2006) First-principles calculations of AlN nanowires and nanotubes: atomic structures, energetics, and surface states. J Phys Chem B 110:8764–8768. https://doi.org/10.1021/jp056755f
26. Becke AD (1993) Density-functional thermochemistry. III. The role of exact exchange. J Chem Phys 98:5648–5652. https://doi.org/10.1063/1.464913
27. Erba A, Baima J, Bush I, Orlando R, Dovesi R (2017) Large-scale condensed matter DFT simulations: performance and capabilities of the CRYSTAL code. J Chem Theory Comput 13:5019–5027. https://doi.org/10.1021/acs.jctc.7b00687
28. Montanari B, Civalleri B, Zicovich-Wilson CM, Dovesi R (2006) Influence of the exchange-correlation functional in all-electron calculations of the vibrational frequencies of corundum (α-Al_2O_3). Int J Quantum Chem 106:1703–1714. https://doi.org/10.1002/qua.20938
29. Pandey R, Jaffe JE, Harrison NM (1994) Ab initio study of high pressure phase transition in GaN. J Phys Chem Solids 55:1357–1361. https://doi.org/10.1016/0022-3697(94)90221-6
30. Dovesi R, Causa' M, Orlando R et al (1990) Ab initio approach to molecular crystals: a periodic Hartree–Fock study of crystalline urea. J Chem Phys 92:7402–7411. https://doi.org/10.1063/1.458592
31. Fabris GSL, Marana NL, Longo E, Sambrano JR (2018) Piezoelectric response of porous nanotubes derived from hexagonal boron nitride under strain influence. ACS Omega 10:13413–13421. https://doi.org/10.1021/acsomega.8b01634
32. Marana NL, Casassa S, Longo E, Sambrano JR (2016) Structural, electronic, vibrational, and topological analysis of single-walled zinc oxide nanotubes. J Phys Chem C 120:6814–6823. https://doi.org/10.1021/acs.jpcc.5b11905
33. Marana NL, Albuquerque AR, La Porta FA et al (2016) Periodic density functional theory study of structural and electronic properties of single-walled zinc oxide and carbon nanotubes. J Solid State Chem 237:36–47. https://doi.org/10.1016/j.jssc.2016.01.017
34. Fabris GSL, Marana NL, Longo E, Sambrano JR (2018) Porous silicene and silicon graphenylene-like surfaces: a DFT study. Theor Chem Acc 137:13. https://doi.org/10.1007/s00214-017-2188-6
35. Marana NL, Casassa SM, Sambrano JR (2017) Piezoelectric, elastic, infrared and Raman behavior of ZnO wurtzite under pressure from periodic DFT calculations. Chem Phys 485–486:98–107. https://doi.org/10.1016/j.chemphys.2017.02.001
36. Hirshfeld FL (1977) Bonded-atom fragments for describing molecular charge densities. Theor Chim Acta 44:129–138. https://doi.org/10.1007/BF00549096
37. Zicovich-Wilson CM, Hô M, Navarrete-López A, Casassa SM (2016) Hirshfeld-I charges in linear combination of atomic orbitals periodic calculations. Theor Chem Acc 135:188. https://doi.org/10.1007/s00214-016-1942-5
38. Schulz H, Thiemann KH (1977) Crystal structure refinement of AlN and GaN. Solid State Commun 23:815–819. https://doi.org/10.1016/0038-1098(77)90959-0
39. Mazini MC, Sambrano JR, Cavalheiro AA, da Silva JHD, Leite DMG (2010) Efeitos da Adição de Átomos de Mn na Rede do Gan via Métodos de Estrutura Eletrônica. Quim Nova 33:834–840. https://doi.org/10.1590/S0100-40422010000400013
40. Smith AR, Feenstra RM, Greve DW, Shin MS, Skowronski M, Neugebauer J, Northrup JE (1999) GaN (0001) surface structures studied using scanning tunneling microscopy and first-principles total energy calculations. Surf Sci 423:70–84. https://doi.org/10.1016/S0039-6028(98)00903-0
41. Northrup JE, Neugebauer J (1996) Theory of GaN ($10\bar{1}0$) and ($11\bar{2}0$) surfaces. Phys Rev B. https://doi.org/10.1103/physrevb.53.r10477
42. Sai N, Mele EJ (2003) Microscopic theory for nanotube piezoelectricity. Phys Rev B. https://doi.org/10.1103/physrevb.68.241405
43. Tu ZC, Hu X (2006) Elasticity and piezoelectricity of zinc oxide crystals, single layers, and possible single-walled nanotubes. Phys Rev B. https://doi.org/10.1103/physrevb.74.035434